Creation and annihilation of non-volatile fixed magnetic skyrmions using voltage control of magnetic anisotropy

Dhritiman Bhattacharya[1], Seyed Armin Razavi[2], Hao Wu[2], Bingqian Dai[2], Kang L. Wang[2*] and Jayasimha Atulasimha[1, 3*]

[1]*Dept. of Mechanical and Nuclear Engineering, Virginia Commonwealth University, Richmond, VA 23284, USA*

[2]*Dept. of Electrical and Computer Engineering, University of California, Los Angeles, CA 90095, USA*

[3]*Dept. of Electrical and Computer Engineering, Virginia Commonwealth University, Richmond, VA 23284, USA*

*Corresponding authors: wang@seas.ucla.edu and jatulasimha@vcu.edu

Abstract: Magnetic skyrmions are topological spin textures that could be used to implement magnetic memory and logic devices. Such devices typically rely on current-controlled motion of skyrmions; but utilizing skyrmions that are fixed in space could lead to more compact and energy efficient devices. Here we report the manipulation of fixed magnetic skyrmions using voltage controlled magnetic anisotropy. We show that skyrmions can be stabilized in antiferromagnet/ferromagnet/oxide heterostructure films without any external magnetic field due to an exchange bias field. The isolated skyrmions are annihilated or formed by applying voltage pulses that increase or decrease the perpendicular magnetic anisotropy, respectively. We also show skyrmions can be created from chiral domains by increasing the perpendicular magnetic anisotropy of the system. Our experimental findings are corroborated using micromagnetic simulations. This could provide a pathway to realize of fixed skyrmion based high density and energy efficient magnetic memory devices.

Following the first experimental observation in bulk MnSi [1], magnetic skyrmion related research has experienced a remarkable growth over the last decade. Due to its topological spin structure, magnetic skyrmions have significantly lower depinning current compared to domain walls [2]. This has motivated exploration of skyrmion motion based implementation of racetrack memory as well as logic devices and several studies were performed to understand the skyrmion dynamics that could lead to successful implementation of such devices [3-18]. However, racetrack based devices, whether realized with domain walls or skyrmions, may necessitate larger footprint to accommodate domain wall/skyrmion motion. On the other hand, manipulation of static (not moving) isolated magnetic skyrmions could lead to more compact memory devices.

As spin spiral structures such as magnetic skyrmions are stabilized due to a balance of Perpendicular Magnetic Anisotropy (PMA) and Dzyaloshinskii-Moriya Interaction (DMI) [19,20], one can expect to induce a magnetic state change via tuning this balance between PMA and DMI. One way to achieve such tuning can be adjusting the PMA of the system employing Voltage Control of Magnetic Anisotropy (VCMA) [21,22]. This occurs as application of an electric field modifies the electron density at ferromagnet/oxide interface, which consequently changes the PMA [21]. Skyrmion creation, annihilation, reversal as well as skyrmion mediated ferromagnetic reversal in confined geometries by modulating PMA through the application of a voltage were previously shown using micromagnetic simulations [23-26]. This mechanism could potentially allow skyrmion states to be manipulated in confined geometries, such as the free layer of a magnetic tunnel junction (MTJ). It could thus be used to achieve non-volatile skyrmion based magnetic memory, where deterministic switching is achieved by applying voltages of appropriate pulse width [23], and experimental work using nanosecond pulsed voltages has recently been reported [27]. These results suggest that skyrmion and skyrmion-mediated ferromagnetic reversal using VCMA can be used to implement memory devices where the switching error is extremely robust to defects and thermal noise. Furthermore, the energy required for skyrmion reversal has been shown to be 2.4 fJ [24] and skyrmion-mediated switching of ferromagnets can be as low as 0.6 fJ [23].

Voltage control of skyrmions has also been experimentally investigated. A scanning probe microscope tip was, for example, used to modify exchange interaction in an iron monolayer to create skyrmions at very low temperatures and high magnetic fields [28]. It has also been shown that room temperature skyrmion nucleation and annihilation can be achieved, by, primarily, changing the saturation magnetization due to changes in Curie temperature caused by the application of an electric field [29]. With this approach, the number of skyrmions varied as a function of electric field in a volatile manner. Room temperature creation and movement of skyrmion bubbles have also been demonstrated when domain walls are moved in an electric field-induced magnetic anisotropy gradient due to geometric effects [30].

In this article, we report voltage control of skyrmions that are fixed in space and stabilized without any external magnetic field. The skyrmions can be annihilated by applying a negative voltage pulse and created by applying a positive voltage pulse. Furthermore, we show that skyrmions can be created from chiral domains. Once created, the skyrmion/ferromagnetic states are non-volatile and do not change when the applied electric field is removed. We also corroborate our experimental findings using micromagnetic simulations. Our approach could lead to the development of memory devices based on manipulation of skyrmion states in confined geometries such as a free layer of a Magnetic Tunnel Junction (MTJ). These devices could also potentially offer lower write error rates compared with conventional VCMA-induced switching and could be two orders of magnitude more energy efficient than spin-transfer torque based

switching [23]. Voltage control of skyrmions could also be applied in areas such as skyrmion-based neuromorphic devices [31-35] and spintronic nano-oscillators [36,37].

Device structure and characterization:

The heterostructure used in our experiments is Ta (2) / IrMn (5) / CoFeB (0.52-1.21) / MgO (2.5) / Al_2O_3 (35) / ITO where the numbers represent the thicknesses in nm. Details of fabrication procedure can be found in the methods section. The interface of CoFeB with the antiferromagnetic IrMn layer gives rise to DMI [38, 39]. Similar to conventional VCMA induced switching, ferromagnetic/oxide interface is used to achieve the necessary PMA as well as enable VCMA. Across the wafer, an array of several hall bars (130 μm ×20 μm) was fabricated (Fig. 1(a)). The thickness of the CoFeB layer was varied across the wafer roughly between 0.52 nm to 1.21 nm. The magnetic properties of the devices, especially the PMA and the DMI, are expected to vary with the thickness of the CoFeB layer. To verify this, anomalous hall resistance due to Anomalous Hall Effect (AHE) was measured to estimate the magnetization component perpendicular to the film as a function of perpendicular magnetic field. This is shown in Fig. 1(b), where the hysteresis loops obtained show the expected trend. For example, devices in the range of 0.87 nm - 1.1 nm CoFeB layer exhibit higher perpendicular anisotropy and abrupt switching, while devices with thickness on either side of this range showed lower perpendicular anisotropy and gradual transition during reversal. Another important observation is the presence of exchange bias field in all the devices (5-20 Oe) that emerges from the ferromagnet/antiferromagnet interface. While presence of PMA and DMI are adequate, an external bias magnetic field is generally required to stabilize skyrmions in experiments. However, in our structure, the readily available interfacial exchange bias field eliminates this requirement thus allowing stabilization of skyrmions at zero externally applied bias magnetic field [38].

The thickness dependence of magnetic states was imaged using Magnetic Force Microscopy (MFM). (We note that, raw MFM images were processed using a Gaussian filter to aid visualization by eliminating noise. The raw images are shown in the supplementary section 5.) In devices with high perpendicular anisotropy, the magnetization orientation was found to be completely out of plane (t=1.092 nm, Fig. 1(c) top panel, we note that stripe like contrasts appear due to optical interference between the laser reflected from the cantilever and the sample surface). In devices with increased thickness, we observed a mixture of stripe domains and circular domains (t=1.126 nm, Fig. 1(c) middle panel) and mostly circular domains (t=1.143 nm, Fig. 1(c) bottom panel). Fig. 1 (d) shows a phase profile extracted from the experimental MFM image of an observed domain along the line shown in the inset. This profile qualitatively matches the simulated MFM profile (Fig. 1(e)) of a skyrmion stabilized in the presence of thermal noise and inhomogeneity (Fig. 1(f)) and is fundamentally different from MFM profile of a classical bubble (see supplementary section 1

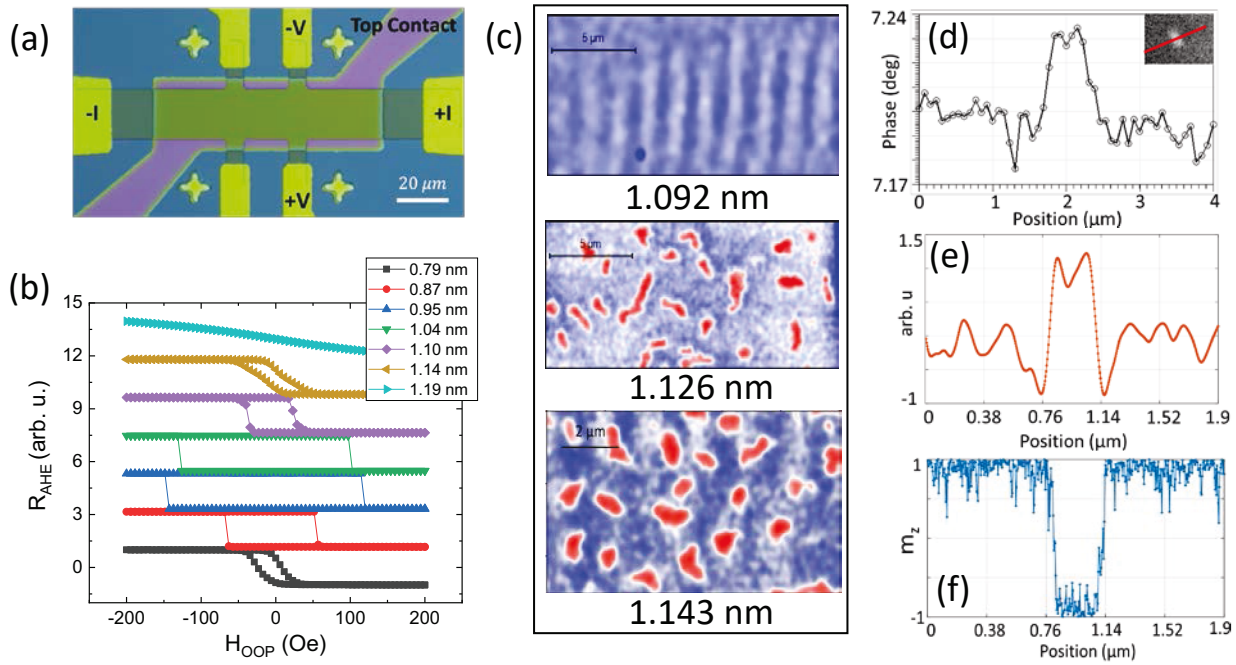

Figure 1. Device structure and characterization. (a) Device structure: The two current contacts can be used for applying current through the stack and the voltage contacts can be used for measuring transverse voltage. For VCMA, a voltage pulse was applied between one of the two top gate contacts, and any one of the other current and voltage contacts. (b) Anomalous Hall measurements for different CoFeB thicknesses, where H_{OOP} denotes out-of-plane magnetic field, (c) Magnetic force microscopy image showing magnetic states for different CoFeB thicknesses. At lower thickness uniform state was observed while at higher thicknesses skyrmions and a mixture of skyrmion and stripe domains were seen. (d) Skyrmion profile obtained from the raw MFM image of a skyrmion shown in the inset which was qualitatively similar to the simulated skyrmion MFM profile as shown in (e). This profile was obtained simulating the skyrmion shown in (f).

for more detailed analysis). These give us confirmation of the presence of skyrmions in our system. The skyrmion has a collinear core at the center. The dip at the center of the MFM profile is indicative of that. Such textures are often called skyrmion bubbles. In a strict sense, spins in a skyrmion structure should rotate continuously with a single spin at the center pointing perpendicularly. However, there is no clear distinction between the skyrmion and the skyrmion bubble state and these terms are used interchangeably in the literature [9, 10]. Lastly, we note that, the observed stripe domain like states are expected to be topologically equivalent to the circular skyrmionic state. Therefore, these states are possibly elongated skyrmions or elliptically shaped skyrmions. However, to avoid confusion we call the mixed state as "skyrmions and stripe domains".

The MFM imaging was further complemented with magneto optical Kerr effect (MOKE) imaging. Skyrmions and stripe domains were clearly observed in the intermediate steps of the switching during a cycle of perpendicular magnetic field as shown in supplementary Video 1. More importantly, we show that

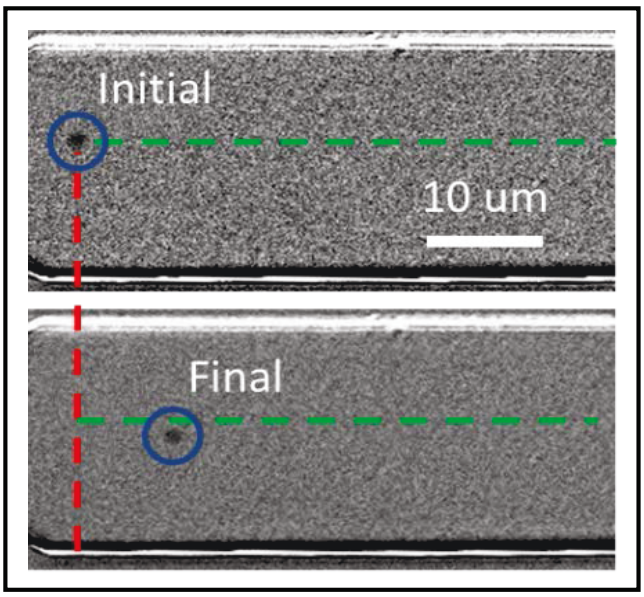

Figure 2. Current-driven skyrmion motion imaged using magneto-optical Kerr effect (MOKE) microscopy. Current pulse has 9 mA amplitude (corresponding to a current density of 8.3×10^6 A/cm^2 through the IrMn layer) and a duration of 5 ms. Blue circles indicate the position of skyrmions before and after the application of current pulse. Red (green) dashed line shows the initial horizontal (vertical) position of the skyrmion. At the final position, the skyrmion also shows a vertical shift in addition to the horizontal one, which is due to the skyrmion Hall effect.

current induced motion of these magnetic objects exhibited skyrmion Hall Effect, which is a clear indication of the topological nature of these magnetic objects. We utilize spin-orbit torques from IrMn (with a thickness of 5 nm) to drive the skyrmion motion [38]. It has been shown that IrMn has a sizable spin Hall angle [40], allowing for a relatively large damping-like spin-orbit torque. First, we create skyrmions by scanning the external magnetic field, and then by utilizing electrical current in this system, we displace skyrmions by pulses with an amplitude of 9 mA and a duration of 5 ms. As seen in Fig. 2, the direction of the current-driven skyrmion motion is not along the current direction and has a transverse component. This phenomenon is the so-called skyrmion Hall effect [9], which is a signature of magnetic skyrmions. The calculated skyrmion Hall angle is around 10.4^o. These results further confirm that our observed states have a topological nature and are indeed skyrmions.

Manipulation of skyrmions with electric field alone in the absence of an external magnetic field: We probe the effect of application of an electric field in the devices where skyrmions and stripe domains were observed at zero magnetic field. A voltage pulse is applied between one of the two top gate contacts, and any one of the other current and voltage contacts. Current and voltage contacts are all attached to the Hall bar, which is .[metallic and conductive. In this way, the electric field is dropped over the MgO and Al_2O_3. Consequently, the electron density at the ferromagnet/oxide interface is modulated, leading to a modulation in the PMA of the system. We characterize VCMA coefficient in our perpendicularly magnetized samples by measuring anomalous Hall resistance as a function of an in-plane magnetic field in our Hall bar structures with top gates. We can then calculate the interfacial anisotropy using the transport data and magnetization

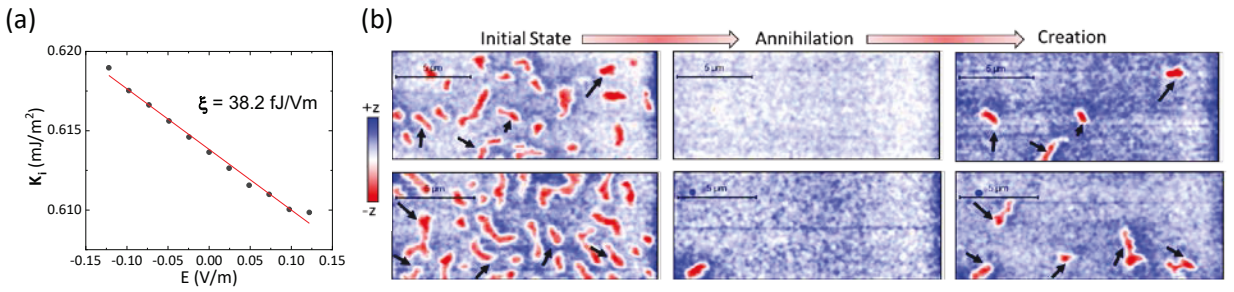

Figure 3. VCMA induced manipulation of skyrmions. (a) Interfacial anisotropy (Ki) as a function of the applied electric field (E) in the sample with nominal CoFeB thickness of 1.06 nm. The slope of this plot is the VCMA coefficient (ξ). (b) MFM images obtained before and after application of electric field. Scale bars are 5 μm. Left column: magnetization state before application of any electric field. Middle Column: Magnetization state obtained after applying a negative voltage pulse that increased PMA. Right Column: Magnetization state obtained after applying a positive voltage pulse that decreased PMA.

saturation obtained from SQUID measurement ($\sim 9\times10^5 \pm 5\%$) A/m [41]. The results are shown in Fig. 3(a), where interfacial anisotropy is plotted as a function of applied electric field. VCMA coefficient (ξ) is defined as the slope of this plot. The effect of voltage application is primarily limited to changing the perpendicular magnetic anisotropy of the system. In other words, applied voltage does not alter the saturation magnetization, exchange bias etc. This is further discussed in supplementary section 2. The oxide barrier breakdown voltage was observed to be around 8 V. In most of the cases, we applied ±7 V across the oxide barrier (unless otherwise mentioned) by using a Keithley 2636B source meter and Signatone probe station, which corresponds to an electric field of $E_{MgO} = \frac{V}{t_{MgO}+\frac{\epsilon_{MgO}}{\epsilon_{AlOx}}t_{AlOx}} = 0.157$ V/nm, using $\frac{\epsilon_{MgO}}{\epsilon_{AlOx}} = \frac{9}{7.5}$.

In our system, application of a positive (negative) electric field leads to decrease (increase) of the PMA (Fig. 3(a)). Before applying this electric field, we imaged the initial magnetization state of the device as shown in the left column of Fig. 3 (b). The initial states consist of skyrmions and stripe domains. Next, we applied -7 V between the top and the bottom electrode for 1-2 seconds to increase the PMA of the system. The voltage pulse was withdrawn and the transformation of the magnetic state due to application of this voltage pulse was imaged in the absence of an applied electric field. We observed that the skyrmions and the stripe domains were annihilated (middle column of Fig. 3(b)) and the magnetization of the system reoriented in the +z direction as evidenced by the MFM image. Subsequently, we applied an opposite polarity voltage pulse (i.e. +7V) in a similar manner. Due to this, the PMA decreases and DMI prevails over PMA. This is expected to be a favorable condition for formation of spin spiral states. Indeed, some skyrmions and stripe domains reappear as can be seen in the MFM images shown in the right column of Fig. 3(b). We note that all imaging was performed at zero external magnetic field and zero applied electric field. Therefore, these creation and annihilation processes were nonvolatile and were achieved without the assistance of any external bias magnetic field. Therefore, the skyrmion state and the saturated out of plane

ferromagnetic state both emerged as stable states of the system and the applied electric field can result in switching between these states.

Additionally, we observed incomplete annihilation where starting from an initial state with mostly stripe domains and some skyrmions; a negative voltage pulse could annihilate some of the skyrmions while many of the stripe domains transformed to more circular skyrmionic state as shown in Fig 4. Therefore, transformation from stripe domain to skyrmions is also achievable using VCMA. However, unlike the previous case, this transformation was found to be irreversible. In other words, application of a positive

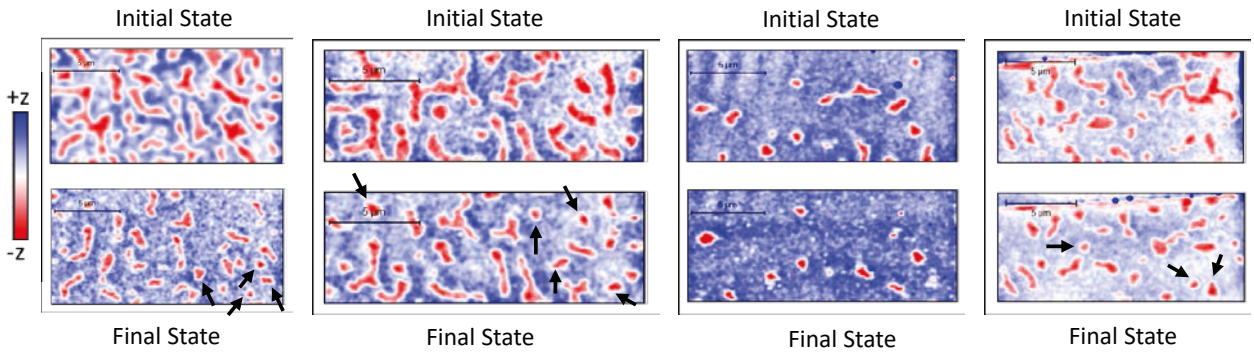

Figure 4. Incomplete annihilation that shows stripe domain to skyrmion transformation. Initial states are shown in the top panel and final state is shown in the bottom panel. Arrows mark some of the created skyrmions due to application of a negative voltage pulse. Scale bars are 5μm.

pulse could not recreate more skyrmions or transform the circular skyrmions back to original stripe domains. Possibly, when the stripe domains transform to circular skyrmions they get pinned more strongly. Therefore, subsequent application of a positive pulse (i.e. reduction of PMA) did not affect them substantially. Transformation from chiral domain to skyrmions were previously observed experimentally by using a current pulse [6,7]. Theoretically, chopping skyrmions from chiral domain was proposed using strain using anisotropy modulation [42]. Here, we demonstrate the feasibility of such transformation by employing VCMA.

All these different observations can be satisfactorily explained if we consider pinning sites in the thin film stack. The CoFeB and the IrMn films are polycrystalline in nature, which could lead to intergranular variation of PMA, DMI and exchange bias. Pinning sites could also exist due to inhomogeneity in film thickness and presence of material defects etc. We observed the size and shape of the skyrmions vary widely (Fig. 1(c)) which indicate the existence of inhomogeneity. Due to corresponding non-uniformity of magnetic parameters across the film, the stripe domains and the skyrmions have a propensity to occupy the same location (e.g. emerge roughly at the same position in successive magnetization cycles, supplementary section 3). Similarly, skyrmions created by VCMA appear at the same initial location that they occupied before annihilation as indicated by the arrows in the Fig. 3(b). The same skyrmions were also present at the

same location in all the magnetization cycles (see supplementary Fig. S3). Finally, due to the pinning sites, fewer skyrmions were created by VCMA compared to the initial state (prior to annihilation) as shown in Fig. 3(b). In the next section, we establish the validity of these explanations using micromagnetic simulation.

Simulations for manipulation of skyrmions with electric field: We perform micromagnetic simulation to show the voltage-controlled creation and annihilation process of skyrmions. Details of the simulation procedure and parameters used can be found in the methods section. For simplicity, we incorporate the effect of inhomogeneity by varying only the perpendicular anisotropy. We simulated a 3.8 μm × 3.8 μm rectangular geometry with 1.1 nm thickness and divided it into regions of average 100 nm size using Voronoi tessellation with a gaussian PMA distribution with 1% standard deviation. Left column of Fig. 5(a) shows the PMA distribution in different regions across the film. Usually, grain size in CoFeB is in the order of 5-10 nm. However, regions of such dimensions were not sufficient to pin skyrmions and consequently corresponding simulations did not reproduce all the experimentally observed scenarios. Ultimately, there can be many causes of inhomogeneity besides intergranular variations. Regions in the film (comprised of many grains) can have exchange bias, PMA, DMI that are clearly different from surrounding areas, particularly in IrMn/CoFeB interfaces. Additionally, there can be material defects in the sample acting as pinning sites. Thus, our systematic study of effect of spatial dimensions of the inhomogeneity indicates that regions that are on average ~100 nm and higher are most effective in pinning skyrmions.

As previously discussed, applied voltage does not alter the saturation magnetization, exchange bias. There are recent reports of DMI modulation by applying an electric field [43]. However, these changes in DMI are relatively small and do not affect the magnetization dynamics significantly [23]. Therefore, we only consider the change in PMA as a consequence of voltage application which is considered to be the same in all the regions. VCMA coefficient in 1.06 nm CoFeB was measured to be 38.2 fJ/Vm (Fig. 3(a)). Therefore, electric field of 0.157 V/nm can cause 5.5×10^3 J/m^3 change in anisotropy energy density. In our simulations, we considered a change of 7×10^3 J/m^3 in anisotropy density, which is close to the estimated change in anisotropy energy density.

Fig. 5(b) shows the overview of the switching process. The initial magnetic state (Fig. 5(b), left column) was obtained by finding the equilibrium magnetization orientation starting from a random magnetization state. During this initialization, a labyrinth like state is first formed which then transforms into many skyrmions and stripe domains. Most of these skyrmions remain pinned due to prevalence of pinning sites of varying strength across the film. These skyrmions were annihilated when PMA was increased and a ferromagnetic state was formed (Fig. 5(b), middle column). Lastly, when PMA was reduced some skyrmions were created at the same initial location that they occupied before annihilation (marked by

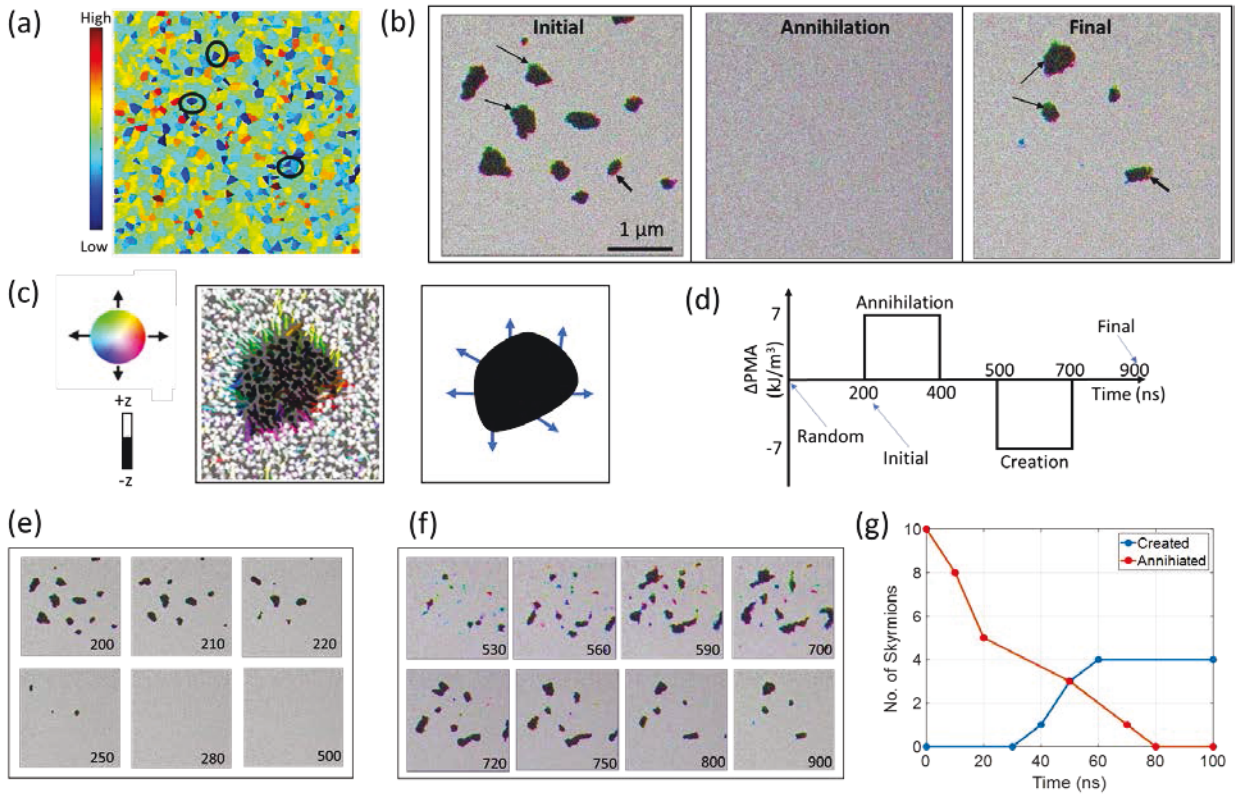

Figure 5. Micromagnetic simulation of voltage control of skyrmions. (a) Simulated system with different regions having a gaussian PMA distribution. The blue regions correspond to lower anisotropy and these act as pinning sites. (b) Overview of the creation and annihilation process. Left column shows equilibrium magnetic state obtained by finding the equilibrium state starting from a random magnetic state. Middle Figure shows the annihilated state while the right figure shows created skyrmions. Arrows show that the skyrmion located at the same pinning site before annihilation and after creation. These pinning sites corresponds to the low anisotropy (blue) regions marked by circles in (a). (c) Zoomed view of a skyrmion (left) with Neel like spin spiral, (d) Temporal PMA variation used in the simulation. (e) Annihilation process of skyrmion. (f) Creation process of skyrmions. The numbers represent time corresponding to the pulse shown in (d), (g) Pulse time dependence of skyrmion creation and annihilation process.

arrows in the Fig. 5(b)). We found that these locations are the low anisotropy regions of the film which act as pinning sites to the skyrmions. Fig. 5(c) shows zoomed in view of a skyrmion. We observe that the skyrmion is Neel like. This is expected as the heterostructure fabricated has interfacial DMI.

Next, we analyze the dynamics of the switching process. As large pulse times (several seconds) were used in the experiment, we ran the simulations with long enough pulse time (200 ns) beyond which increasing pulse time makes no difference. The pulse used in our simulation is shown in Fig. 5(d) where increase (decrease) of PMA correspond to a negative (positive) voltage. Fig. 5(e) shows the annihilation process starting from the initial state. Due to increase of PMA, skyrmions start to shrink and ultimately annihilates. At t=280 ns, all the skyrmions are annihilated and a ferromagnetic state is reached. This ferromagnetic state persists when the PMA is restored to the original value (t=400-500 ns). Fig. 5(f) shows the creation process

starting from a ferromagnetic state. Due to PMA reduction, domains start to nucleate at regions of low PMA. Domain growth slows down over time and almost entirely stops at t=700 ns. When the PMA is restored to the initial value, some of these domains start to annihilate. However, after 200 ns (t=900 ns), 4 skyrmions still persist. Clearly, number of created skyrmions are fewer than the initial state. This is because, starting from a ferromagnetic state, domains nucleate only at very strong pinning sites when PMA is reduced. However, when skyrmions are formed from a labyrinth like state (which is observed in our initialization process), many skyrmions can interact with comparatively lower strength pinning sites and remain pinned there. This explains the creation of fewer skyrmions compared to the initial state. It was previously shown using a magnetic field, more skyrmions can be created from a labyrinth domain state than from a single domain saturated state due to non-uniformity [38] which is consistent with our simulation and experimental observations. Finally, we explore the pulse time dependence of skyrmion creation and annihilation process. We show in Fig. 5 (g), the switching can be controlled by varying the pulse time and 80 ns is enough for both annihilation as well as creation of skyrmions.

Estimation of energy dissipation: We estimate the total energy dissipation considering all the energy required to charge the capacitive oxide layer is ultimately dissipated. The capacitance of the 130 µm × 20 µm area with 35 nm Al_2O_3 layer and 2.5 nm MgO layer is C= 4.66×10^{-12} F (relative permittivity of 9 and 7.5 respectively). Therefore, total energy dissipation= $\frac{1}{2}CV^2$= 109 pJ as V=7 V. Initially, the density of chiral objects (Skyrmions and stripe domains) observed in our devices was 0.183 μm^{-2}. Therefore, the total number of such objects in a 130 µm× 20 µm area is expected to be around 660. Thus, the energy required to annihilate each object (skyrmion or stripe domain) on an average =166 fJ. On the other hand, number of created Skyrmions is fewer than the initial condition with a density of 0.03 μm^{-2}. This translates into average energy dissipation to create a skyrmion = 995 fJ. We note that the oxide barrier was grown thicker compared to a patterned MTJ to avoid pinholes. In a scaled device, MgO thickness will usually be 1.5 nm. That will provide a reduction in the energy dissipation by a factor of 25 and the energy dissipated will be much lower (~6.6 fJ for annihilation, ~40 fJ for creation). Furthermore, interface optimization can lead to a higher VCMA co-efficient. For example, a VCMA co-efficient of 100 $\mu J/m^2$ per V/nm [41] can reduce the energy dissipation to ~1 fJ for annihilation, ~6 fJ for creation. Finally, these proof-of-concept experiments were performed with large skyrmions. If skyrmion diameter is ~100 nm, the energy dissipated could potentially be much smaller than 1 fJ/skyrmion creation or annihilation event.

Conclusion: We have reported control of fixed magnetic skyrmions using VCMA. In particular, we showed that skyrmions can be stabilized without applying any external magnetic field and can be annihilated and recreated by applying voltages of opposite polarity. We also showed that skyrmions can be created from

chiral domain states. This control is non-volatile and depends on the pinning sites across the device. Our experimental observations were corroborated using micromagnetic analysis. The electric field control of magnetic skyrmions could lead to the development of energy efficient high-density magnetic memory devices.

Methods

Fabrication/MOKE/Transport:

The layers consisting of Ta (2) / IrMn (5) / CoFeB (0.52-1.21) / MgO (2.5) / Al_2O_3 (5) were grown on Si/SiO_2 substrates by DC and RF magnetron sputtering at room temperature, where the numbers represent the thicknesses in nm. The CoFeB layer has a wedge shape with continuously changing thickness with a gradient of 0.115 nm per 1 cm of the sample length. The samples were then patterned into an array of Hall bar devices using standard photolithography techniques. A 30 nm Al_2O_3 gate oxide was deposited using atomic layer deposition (ALD), and ITO layers were fabricated as a top gate electrode. The samples were then annealed at 150^o C for 30 minutes under an out-of-plane magnetic field of 6 kOe to introduce the exchange bias and enhance the perpendicular anisotropy. The dimensions of the Hall bars are $130\ \mu m \times 20\ \mu m$. All electrical and optical measurements were done at room temperature using Keithley 6221 current source, Keithley 2182A nanovoltmeter, Stanford Research Systems SR830 lock-in amplifier, and HeNe laser with 632.8 nm of wavelength. The external magnetic field is provided by an electromagnet driven by a Kepco power supply.

Magnetic Force Microscopy:

We obtained MFM image at room temperature and atmospheric pressure with Bruker Dimension Icon AFM system. We used Bruker MESP-LM low-moment probes to minimize tip-induced magnetization reorientation. To confirm there is no tip induced effects, we scanned the same area twice (scanning up and down). These two scans produced similar images (see supplementary section 4). Nominal cantilever frequency, lift height and scan rate were respectively 75 kHz, 40 nm and 0.2 Hz.

Micromagnetic Simulation:

Micromagnetic simulation software-Mumax3 [44] was used to perform the simulations where the magnetization dynamics is simulated using the Landau-Lifshitz-Gilbert (LLG) equation:

$$\frac{\partial \vec{m}}{\partial t} = \vec{\tau} = \left(\frac{-\gamma}{1+\alpha^2}\right)\left((\vec{m} \times \vec{H}_{eff}) + \alpha\left(\vec{m} \times (\vec{m} \times \vec{H}_{eff})\right)\right)$$

Here $\vec{m}$ is the reduced magnetization ($\vec{M}$/M_{sat}), M_{sat} is the saturation magnetization, γ is the gyromagnetic ratio and α is the Gilbert damping coefficient.

The quantity H_{eff} is the effective magnetic field, which includes the effective field due to demagnetization energy, exchange bias, Heisenberg exchange coupling and DMI interaction, and perpendicular magnetic anisotropy (PMA).

$$\vec{H}_{eff} = \vec{H}_{demag} + \vec{H}_{exch\_bias} + \vec{H}_{exchange} + \vec{H}_{anis}$$

H_{anis} is the effective field due to the perpendicular anisotropy

$$\vec{H}_{anis} = \frac{2K_{u1}}{\mu_0 M_s}(\vec{u}.\vec{m})\vec{u} + \frac{4K_{u2}}{\mu_0 M_s}(\vec{u}.\vec{m})^3$$

where, K_{u1} and K_{u2} are first and second order uniaxial anisotropy constants and $\vec{u}$ is the unit vector in the direction of the anisotropy (i.e. perpendicular anisotropy in this case). VCMA effectively modulates the anisotropy energy density, which is given by $\Delta PMA = \xi E$. Here ξ and E are respectively the coefficient of electric field control of magnetic anisotropy and the applied electric field. The resultant change in uniaxial anisotropy due to VCMA is incorporated by modulating K_{u1} while keeping $K_{u2} = 0$. Material parameters used in the simulation: saturation Magnetization (Ms)= 9.3×10^5 A/m (measured by SQUID= 9×10^5 ±5% A/m), Perpendicular Anisotropy Constant (Ku_1) = 5.8×10^5 J/m^3 (Fig. 3a), Exchange Bias=15 Oe (Fig. 1b), Exchange Constant (A)=8 pJ/m [45], DMI Parameter (D)=135 μJ/m^2 [39], Gilbert Damping (α)=0.01.

Supporting Information: Detailed analysis of MFM profile, exchange bias and M_s dependence on gate voltage, emergence of skyrmion/stripe domains at same location in different magnetization cycle, Up and Down MFM Scan, raw MFM images and Micromagnetic code.

Data Availability Statement: All MFM datafiles used in this manuscript are available at https://doi.org/10.6084/m9.figshare.12234446

References:

[1] Pfleiderer C, Rosch A, Neubauer A and Georgii R, Skyrmion Lattice in a Chiral Magnet *Science* ***323,*** 915–20 (2009).

[2] Jonitez F. et al Spin Transfer Torques in MnSi at Ultralow Current Densities Science Vol. 330, Issue 6011, pp. 1648-1651 (2010).

[3] Fert A, Cros V and Sampaio J, Skyrmions on the track *Nat. Nanotechnol.* **8,** 152–6 (2013).

[4] Tomasello R, Martinez E, Zivieri R, Torres L, Carpentieri M and Finocchio G A strategy for the design of skyrmion racetrack memories, *Sci. Rep.* **4,** 6784 (2014).

[5] Mochizuki M, Yu X Z, Seki S, Kanazawa N, Koshibae W, Zang J, Mostovoy M, Tokura Y, Nagosa N, Thermally driven ratchet motion of a skyrmion microcrystal and topological magnon Hall effect, *Nat. Mater.*, **13**, 241 (2014).

[6] Jiang W, Upadhyaya P, Zhang W, Yu G, Jungfleisch M B, Fradin F Y, Pearson J E, Tserkovnyak Y, Wang K L, Heinonen O, te Velthuis S G E and Hoffmann A, Blowing magnetic skyrmion bubbles *Science* **349,** 283–6 (2015).

[7] Yu G, Upadhyaya P, Shao Q, Wu H, Yin G, Li X, He C, Jiang W, Han X, Amiri P K and Wang K L, Room-temperature skyrmion shift device for memory application, *Nano Lett.* **17,** 261–8 (2017).

[8] Yu X Z, Kanazawa N, Onose Y, Kimoto K, Zhang W Z, Ishiwata S, Matsui Y and Tokura Y, Near room-temperature formation of a skyrmion crystal in thin-films of the helimagnet FeGe, *Nat. Mater.* **10,** 106–9 (2011).

[9] Jiang W, Zhang X, Yu G, Zhang W, Wang X, Benjamin Jungfleisch M, Pearson J E, Cheng X, Heinonen O, Wang K L, Zhou Y, Hoffmann A and Te Velthuis S G E, Direct observation of the skyrmion Hall effect, *Nat. Phys.* **13,** 162–9 (2017).

[10] Boulle O et al, Room-temperature chiral magnetic skyrmions in ultrathin magnetic nanostructures, *Nat. Nanotech.*, **11**, p. 449 (2016).

[11] Büttner F et al, Field-free deterministic ultrafast creation of magnetic skyrmions by spin–orbit torques, *Nat. Nanotech.*, **12**: p. 1040 (2017).

[12] Caretta L et al, Fast current-driven domain walls and small skyrmions in a compensated ferrimagnet, *Nat. Nanotech.*, **13**(12), 1154-1160 (2018).

[13] Everschor-Sitte K, Sitte M, Valet T, Abanov A, Sinova J, Skyrmion production on demand by homogeneous DC currents, *New J. Phys*. **19**, 092001, (2017).

[14] Litzius K et al, Skyrmion Hall effect revealed by direct time-resolved X-ray microscopy, *Nat. Phys.*, **13**: 170 (2016).

[15] Maccariello D, Legrand W, Reyren N, Garcia K, Bouzehouane K, Collin S, Cros V, and Fert A, Electrical detection of single magnetic skyrmions in metallic multilayers at room temperature, *Nat. Nanotech.*, **13**(3): p. 233-237 (2018).

[16] Moreau-Luchaire C et al, Additive interfacial chiral interaction in multilayers for stabilization of small individual skyrmions at room temperature, *Nat. Nanotech.*, **11**, 444, (2016).

[17] Romming N, Hanneken C, Menzel M, Bickel J E, Wolter B, Bergmann K. von, Kubetzka A, and Wiesendanger R, Writing and Deleting Single Magnetic Skyrmions, *Science*, **341**(6146), 636 (2013).

[18] Woo S et al, Observation of room-temperature magnetic skyrmions and their current-driven dynamics in ultrathin metallic ferromagnets, *Nat. Mater.*, **15**, 501 (2016).

[19] Moriya T, Anisotropic superexchange interaction and weak ferromagnetism, *Phys. Rev.* **120,** 91–8, (1960)

[20] Dzyaloshinsky I, A thermodynamic theory of "weak" ferromagnetism of antiferromagnetics, *J. Phys. Chem. Solids* **4,** 241, (1958).

[21] Shiota Y, Nozaki T, Bonell F, Murakami S, Shinjo T and Suzuki Y Induction of coherent magnetization switching in a few atomic layers of FeCo using voltage pulses. *Nat. Mater.* **11,** 39, (2012).

[22] Amiri P K and Wang K L, Voltage-Controlled Magnetic Anisotropy in Spintronic Devices, *Spin* **2,** 1240002 (2012).

[23] Bhattacharya D and Atulasimha J, Skyrmion-Mediated Voltage-Controlled Switching of Ferromagnets for Reliable and Energy-Efficient Two-Terminal Memory, *ACS Appl. Mater. Interfaces* **10,** 17455–62 (2018).

[24] Bhattacharya D, Al-Rashid M and Atulasimha J, Voltage controlled core reversal of fixed magnetic skyrmions without a magnetic field, *Sci. Rep* **6,** 31272, (2016).

[25] Bhattacharya D, Al-Rashid M M and Atulasimha J, Energy efficient and fast reversal of a fixed skyrmion two-terminal memory with spin current assisted by voltage controlled magnetic anisotropy, *Nanotechnology* **28,** 42 (2017).

[26] Nakatani Y, Hayashi M, Kanai S, Fukami S, and Ohno H, Electric field control of Skyrmions in magnetic nanodisks, Appl. Phys. Lett. **108**, 152403 (2016).

[27] Kasai S, Sugimoto S, Nakatani Y, Ishikawa R, Takahashi Y K, Voltage-controlled magnetic skyrmions in magnetic tunnel junctions, *Appl. Phys. Express* 12 083001 (2019).

[28] Hsu P J, Kubetzka A, Finco A, Romming N, Von Bergmann K and Wiesendanger R, Electric-field-driven switching of individual magnetic skyrmions, *Nat. Nanotechnol.* **12** 123–6 (2017).

[29] Schott M, Bernand-Mantel A, Ranno L, Pizzini S, Vogel J, Béa H, Baraduc C, Auffret S, Gaudin G and Givord D, *Nano Lett.* **17** 3006–12 (2017).

[30] Ma C, Zhang X, Yamada Y, Xia J, Ezawa M, Jiang W, Zhou Y, Morisako A and Liu X, Electric Field-Induced Creation and Directional Motion of Domain Walls and Skyrmion Bubbles, *Nano Lett.* **19 (1)**, pp 353–361(2019).

[31] Azam M A, Bhattacharya D, Querlioz D and Atulasimha J, Resonate and fire neuron with fixed magnetic skyrmions, *Journal of Applied Physics* **124**, 152122 (2018).

[32] Li S, Kang W, Huang Y, Zhang X, Zhou Y and Zhao W, Magnetic skyrmion-based artificial neuron device, *Nanotechnology* 28 31LT01 (2017).

[33] Chen M-C, Sengupta A and Roy K, Magnetic Skyrmion as a Spintronic Deep Learning Spiking Neuron Processor, *IEEE Trans ON MAGNETICS*, VOL. 54, NO. 8, pp 1-7, AUGUST 2018.

[34] Song K M et al, Magnetic skyrmion artificial synapse for neuromorphic computing, arXiv, 1907.00957 (2019).

[35] Pinna D et al. Skyrmion Gas Manipulation for Probabilistic Computing, *Phys. Rev. Applied* 9, 064018 (2018).

[36] Garcia-Sanchez F, Sampaio J, Reyren N, Cros V, Kim J-V, A skyrmion-based spin-torque nano-oscillator, *New J. Phys.* **18** 075011 (2016).

[37] Zhang S, Wang J, Zheng Q, Zhu Q, Liu X, Chen S, Jin C, Liu Q, Jia C and Xue D, Current-induced magnetic skyrmions oscillator, *New J. Phys.* **17** 023061 (2015).

[38] Yu G, Jenkins A, Ma X, Razavi S A, He C, Yin G, Shao Q, He Q L, Wu H, Li W, Jiang W, Han X, Li X, Bleszynski Jayich A C, Amiri P K and Wang K L, Room-Temperature Skyrmions in an Antiferromagnet-Based Heterostructure, *Nano Lett.* **18,** 980–6 (2018).

[39] Ma X, Yu G, Razavi S A, Sasaki S S, Li X, Hao K, Tolbert S H, Wang K L and Li X, Dzyaloshinskii-Moriya Interaction across an Antiferromagnet-Ferromagnet Interface, *Phys. Rev. Lett.* **119,** 027202 (2017).

[40] D. Wu, G. Yu, C.-T. Chen, S.A. Razavi, Q. Shao, X. Li, B. Zhao, K.L. Wong, C. He, Z. Zhang, P.K. Amiri, and K.L. Wang, Spin-orbit torques in perpendicularly magnetized Ir22Mn78/Co20Fe60B20/MgO multilayer. *Appl. Phys. Lett.*, **109**(22): p. 222401, 2016.

[41] X. Li, K. Fitzell, D. Wu, C.T. Karaba, A. Buditama, G. Yu, K.L. Wong, N. Altieri, C. Grezes, N. Kioussis, S. Tolbert, Z. Zhang, J.P. Chang, P.K. Amiri, and K.L. Wang, Enhancement of voltage-controlled magnetic anisotropy through precise control of Mg insertion thickness at CoFeB|MgO interface. *Appl. Phys. Lett.*, 110(5): p. 052401, (2017).

[42] Liu Y, Lei N, Zhao W, Liu W, Ruotolo A, Braun H B and Zhou Y, Chopping skyrmions from magnetic chiral domains with uniaxial stress in magnetic nanowire, *Appl. Phys. Lett.* **111,** 022406 (2017).

[43] Yang H, Boulle O, Cros V, Fert A and Chshiev M, Controlling Dzyaloshinskii-Moriya Interaction via Chirality Dependent Layer Stacking, Insulator Capping and Electric Field, *Sci. Rep.*, **8,** 12356 (2018).

[44] Vansteenkiste A, Leliaert J, Dvornik M, Helsen M, Garcia-Sanchez F and Van Waeyenberge B, The design and verification of MuMax3, *AIP Adv.* **4,** 107133 (2014).

[45] Yamanouchi M, Jander A, Dhagat P, Ikeda S, Matsukura F, and Ohno H, Domain Structure in

CoFeB Thin Films with Perpendicular Magnetic Anisotropy, *IEEE MAGNETICS LETTERS*, Volume 2, 3000304 (2011).

Acknowledgment: D.B. and J.A. are supported in part by NSF CAREER grant CCF-1253370, NSF CCF-1909030 and NSF ECCS 1609303, a VCU Quest Commercialization Grant and a Virginia Microelectronics Seed Grant. S.A.R., H.W., B.D. and K.L.W. are supported by the National Science Foundation (NSF) ECCS 1611570 and NSF Nanosystems Engineering Research Center for Translational Applications of Nanoscale Multiferroic Systems (TANMS). The authors at UCLA are also supported by Spins and Heat in Nanoscale Electronic Systems (SHINES), an Energy Frontier Research Center funded by the US Department of Energy (DOE), Office of Science, Basic Energy Sciences (BES) under award no. SC0012670. The authors at UCLA were also partially sponsored by the Army Research Office under grant no. W911NF-16-1-0472.

Author Contributions: D.B, S.A.R., H.W., K.L.W and J.A. played a role in conception of the idea, planning the experiments, discussing the data, analysing the results and writing the manuscript. D.B performed the MFM and micromagnetic simulations, S.A.R performed other experimental characterization, H.W. fabricated the samples and B.D. performed MOKE. J. A. also coordinated the overall project.

Competing Financial Interests

The authors declare no competing financial interests.